



MiR-20a-5p targets RBM24 and alleviates hypertensive intracerebral hemorrhage

Li Xu, Chuangqi Mo, Ming Lu, Pingping Wang, Yue Liu*

Department of Neurosurgery, Nanjing Pukou People's Hospital, Nanjing, Jiangsu 211800, China

ARTICLE INFO

Original paper

Article history:

Received: June 03, 2023

Accepted: November 09, 2023

Published: December 10, 2023

Keywords:

Hypertensive intracerebral hemorrhage (HICH), miR-20a-5p, RBM24, HIF1 α /VEGFA

ABSTRACT

Hypertensive intracerebral hemorrhage (HICH) poses a significant challenge due to its high incidence, mortality, and diagnostic complexities. The underlying molecular mechanisms of HICH development remain enigmatic. In this study, we identified differentially expressed miRNAs in HICH patients by employing miRNA microarray analysis. We found that miR-20a-5p was one of the miRNAs significantly down-regulated in HICH patients and was significantly associated with clinicopathological features of the patients. Subsequently, Human umbilical vein endothelial cells (HUVECs) were transfected with miR-20a-5p mimics or inhibitors to investigate the role of miR-20a-5p in proliferation, apoptosis, migration, and angiogenesis. Similarly, a mimic of miR-20a-5p or its inhibitor was injected into the HICH animal model and measured HICH markers in brain tissue. We next employed a bioinformatic approach to investigate the potential targets of miR-20a-5p which was further confirmed using gain and loss of function assays in HUVECs and animal models. The results show that overexpression of miR-20a-5p in HUVECs enhanced cell proliferation, migration, and tube formation while suppressing apoptosis, and attenuated HICH development in vivo. miR-20a-5p mediated its effects by directly targeting RBM24 and silencing RBM24 could partially recover the suppressive effects of miR-20a-5p on the development of HICH. Interestingly, miR-20a-5p hindered the development of HICH and its influence relied on the HIF1 α /VEGFA pathway.

Doi: <http://dx.doi.org/10.14715/cmb/2023.69.13.21>

Copyright: © 2023 by the C.M.B. Association. All rights reserved.

Introduction

Hypertensive cerebral hemorrhage (HICH) refers to the spontaneous hemorrhage in the brain parenchyma caused by hypertension or sudden increase in blood pressure (1, 2). HICH has high disability and fatality rate, which causes a heavy burden to individuals, families, and society (3). Therefore, it is of great significance to find effective molecular markers and study their molecular mechanism to provide more effective clinical treatments for HICH.

In recent years, with the development of medical imaging technology and the improvement of neurosurgery treatment, the disability and fatality rate of HICH has decreased, while the pathogenesis and the reasons for the high incidence of HICH are not fully understood. The pathogenesis of HICH is relatively complex, involving multiple factors such as genetics, environment, infection, and immunity, among which hypertension is the most important cause (4, 5). Because intracranial arteries have less middle muscle cells and outer connective tissue and lack outer elastic layer, long-term hypertension can cause hyalinosis, fibrinoid necrosis, and even the formation of microaneurysms or dissecting arteries. This will lead to the blood vessels rupture and cause bleeding when the blood pressure suddenly rises (6, 7). With the rapid development of the advanced study in HICH, several molecular markers have been investigated. COL1A2 rs42524 polymorphism was associated with the development of hypertensive intracerebral hemorrhage, particularly associated with tobacco use and alcohol consumption in the Chinese population (8). Recently, Liu *et al.* demonstrated that NIHSS

score and high-density lipoprotein cholesterol level were prominently higher in HICH patients with CG and GG genotypes of ET-1 gene polymorphism rs1920453 than those in patients with CC genotype, suggesting that Rs1920453 in the promoter region of ET-1 gene was correlated with the occurrence of HICH (9).

MicroRNAs (miRNAs) are endogenous non-coding single-stranded small RNAs with a length of 19-22 nucleotides, which are widely present in the biological world (10). MiRNAs regulate the expression of target genes by fully or partially complementary binding to the 3'UTR regions of target mRNAs (11) and participate in different physiological and pathological processes (12,13). Increasing numbers of studies have demonstrated that miRNAs play crucial roles in intracerebral hemorrhage by regulating various kinds of progress (14). For example, lncRNA Mtss1 promoted inflammatory responses and secondary brain injury after intracerebral hemorrhage by targeting miR-709 in mice (15). Thrombin-induced miRNA-24-1-5p upregulation promoted angiogenesis by targeting prolyl hydroxylase domain 1 in intracerebral hemorrhagic rats (16). Dong *et al.* demonstrated that lncRNA-FENDRR promotes the apoptosis of brain microvascular endothelial cells via regulating miR-126 in mice with HICH (17), suggesting that miRNA might play crucial roles in HICH. However, the key miRNAs in HICH and their mechanisms were not fully understood. Therefore, in the present study, we intend to investigate the key miRNAs in HICH, and the mechanism of the miRNAs involved in the development of HICH.

* Corresponding author. Email: Liuyue6283@163.com

Materials and Methods

Human samples

Human peripheral blood was collected from 33 HICH patients and 27 healthy individuals between 2017 and 2018. The diagnosis of HICH relies on CT imaging diagnosis and a history of hypertension. According to the results of CT examination and the bleeding site, HICH consists of basal ganglia, ventricular, thalamic, brainstem and cerebellar hemorrhage. Patients with trauma, brain tumor, cerebral infarction, vascular malformation, and secondary cerebral hemorrhage caused by other reasons were excluded. There was no significant difference between the two groups of age, gender, and other basic clinicopathological data after statistical analysis ($P > 0.05$).

RNA extraction and miRNA microarray

The peripheral blood of HICH patients ($N=3$) and the healthy controls ($N=3$) were used for miRNA microarray. An RNeasy Mini Kit (74104, QIAGEN) was used to isolate the RNA. The quality and quantity of RNA were measured by NanoDrop. Sample labeling and array hybridization were performed according to the Agilent miRNA Microarray System with miRNA Complete Labeling and Hyb Kit protocol (Agilent Technology). After the hybridized arrays were washed, fixed, and scanned using the Agilent Microarray Scanner, the Agilent Feature Extraction software (version 11.0.1.1) was used to analyze the acquired array images. Quantile normalization and subsequent data processing were performed using the GeneSpring GX v14.9 software package (Agilent Technologies). Differentially expressed miRNAs were identified through Fold Change filtering (Fold Change > 2.0 , FDR < 1.0). R script was used to perform Hierarchical Clustering.

Animal model of hypertensive intracerebral hemorrhage

The C57BL/6 mice at the age of eight months were purchased to establish the HICH model. The mice were housed at room temperature (20–25°C) in a constant humidity (55±5%) with free access to food and water at a regular 12/12-h light/dark cycle. The C57BL/6 mice were randomly divided into experimental and normal groups ($n=20$ for each group).

The experimental group was subcutaneously given angiotensin II (100 mg/kg/day) by a micro-osmotic pump. Meanwhile, these animals were also fed with N-nitro-L-arginine methyl ester (L-NAME 100 mg/kg/day) to construct a mouse model of HICH. The control mice were fed normally for 18 weeks. Animals were observed for any sign of stroke by evaluating blood pressure, behavioral testing, and pathological testing. Blood pressure was measured by a Welch Allyn Pro BP 2000 sphygmomanometer. Behavioral tests were performed three times a day for HICH signs i.e., Contralateral forelimb stretching, hovering, trembling, or other motor dysfunction.

For assessing functions of miR-20a-5p, 20 µg miR-20a-5p mimics or inhibitors were injected into mice via tail vein. For evaluating function of RBM24, lentivirus harboring the full length of RBM24 and si-RNA sequence of RBM24 were injected into mice via tail vein.

Histopathological staining

Brain tissues from different groups were obtained,

fixed with 4% paraformaldehyde, and embedded in paraffin. Brain tissues were sliced into 4 µm sections for hematoxylin-eosin (HE) staining. Briefly, the sections were deparaffinized in xylene, passed through different concentrations of ethanol, rehydrated in water and passed through hematoxylin and eosin, and finally sealed with mounting media. The tissue slices were photographed by a microscope (Olympus, Japan).

Cell culture and treatment

Human umbilical vein endothelial cells (HUVECs) were purchased from The Global Bioresource Center (ATCC). After cell recovery, cells were cultured in the 90% Dulbecco's modified Eagle's medium (DMEM, 12430054, Gibco, USA) supplemented with 10% foetal bovine serum (FBS, Gibco, USA), 100 U/mL penicillin and 100 µg/mL streptomycin at 37°C in a 5% CO₂ incubator under 95% saturation humidity. HUVECs were induced by 1 µmol/L Ang II (Sigma) for 12 h to establish the HICH cell model. HUVECs were seeded in a six-well plate until the confluence reached 70–90%. MiR-20a-5p mimics or inhibitor, pcDNA-RBM24 or RBM24 siRNA was transiently transfected into HUVECs and cultured for 24 h. The miR-20a-5p mimics, inhibitor and NC sequences were synthesized by Shanghai GenePharma Co., Ltd. and sequences were listed as follows: miR-20a-5p mimics: 5'-UAAAGUGCUUAUAGUGCAGGUAGCUACCU-GCACUAUAAGCACUUUA-3'; miR-20a-5p inhibitor: 5'-UAAAGUGCUGACAGUGCAGAU GCGAAGAG-GTGACAGUGCAGA-3'; NC: 5'-GCACCGUCAAGG-CUGAGAACUGGTGAAGACGCCAGUGGA-3'.

Luciferase assay

Fragments of RBM24 3'untranslated regions (UTR) containing the miR-20a-5p binding sites were inserted into the luciferase reporter gene vector pmirGLO. The RBM24-wt or RBM24-mut pmirGLO vectors were delivered into HEK293T cells by Lipofectamine® 3000 (Thermo Fisher) in the presence of miR-20a-5p mimics or inhibitor. The luciferase activity was determined using a dual-luciferase reporter assay system kit (E1910, Promega, USA) according to the manufacturer's instructions. Relative luciferase activity was presented as firefly luciferase relative to that of *Renilla* luciferase.

RNA extraction and quantification

Total RNA was extracted using the RNeasy Mini Kit (Qiagen, Valencia, CA, USA) according to the manufacturer's instructions. cDNA was synthesized from mRNA by using a HiScript II One-Step RT-PCR Kit (Dye Plus) (P612-01, Vazyme, Nanjing, China) and miRNA using a 1st Strand cDNA Synthesis Kit (by stem-loop) (MR101-01, Vazyme, Nanjing, China) following the manufacturer's instructions. Real time quantitative PCR (qRT-qPCR) was performed with the ABI 7500 instrument (ABI, USA) and 20 µL RT-qPCR reaction mixture that contained 9 µL of SYBR Mix, 0.5 µL of each primer (10 µM), 2 µL of the cDNA template, and 8 µL of RNase free H₂O. Thermal cycling parameters for the amplification were as follows: 95°C for 10 min, followed by 40 cycles at 95°C for 15 s, 60°C for 1 min. The miR-20a-5p level was normalized to U6 and the target mRNA level was normalized to GAPDH. Results were calculated by using 2^{-ΔΔCT} method. The primers used in the present study was listed as follows: miR-20a-

5p Forward: 5'-TAAAGTGCTTATAGTGCAGGTAG-3', Reverse: 5'-GCAATGTAGAATCCGCTGGG-3'; U6 Forward: 5'-ACGCAAATTCGTGAAGCGTT-3', Reverse: 5'-CAGTCCAAGTACACAATTCG-3'; CPD5-PL Forward: 5'-CATCCTGAGAATGCAGTGC-3', Reverse: 5'-GAAGAACGGGATGAGGTCC-3'; OPCML Forward: 5'-CATAGTGCAAGTTCCTCCC-3', Reverse: 5'-CATAACAGGGTCACACTGC-3'; RBM24 Forward: 5'-GTCTTCGGAGACATCGAGG-3', Reverse: 5'-CATGGTGACAAATCCGTAGC-3'; Hif-1 α Forward: 5'-TGGTGCTAACAGATGACGG-3', Reverse: 5'-GTGTCCAGTTAGTTCAAAGTCC-3'; VEGFA Forward: 5'-GATCAAACCTCACCAAAGCC-3', Reverse: 5'-TCTTTCTTTGGTCTGCATTCAC-3'; GAPDH Forward: 5'-GCACCGTCAAGGCTGAGAAC-3, Reverse: 5'-TGGTGAAGACGCCAGTGGA-3'.

Western blot

Total protein from HUVECs and brain tissues was extracted using RIPA Lysis Buffer. Protein abundances were determined using the BCA Protein Assay Kit (70-PQ0012, MultiSciences, China) following the manufacturer's instructions. 20 μ g proteins for each sample with protein loading buffer were boiled at 100°C for 5 min, followed by separation in 10-12% SDS-PAGE and transferred onto PVDF membranes. The membranes were then blocked with 5% fat-free milk/TBST buffer for 2 h at room temperature, incubated with anti-CTD5PL (MA5-24798, 1:500, Invitrogen), anti-OPCML (PA5-79772, 1:500, Invitrogen), anti-RBM24 (18178-1-AP, 1:1000, Proteintech), anti-HIF1 α antibody (ab51608, 1:2000), anti-VEGFA antibody (ab183100, 1:450), and anti-GAPDH (ab8245, 1:5000, Abcam, Cambridge, UK) primary antibodies for 2 h at 4°C overnight. After incubation with secondary antibodies anti-mouse IgG (ab205719, 1:20000, Abcam, Cambridge, UK) or anti-rabbit IgG (ab6721, 1:20000, Abcam, Cambridge, UK) for 1-2 h at room temperature and washing by TBST, the immuno-complexes were finally detected by ECL and analyzed using the Image-Pro Plus 6.0 software.

Cell proliferation, migration and tube formation assay

The proliferation of cultured HUVECs with different treatments was measured by the Cell Counting 8 kit (#C0038; Beyotime) following the manufacturer's instructions. Briefly, HUVECs were seeded in the 96-well plates and incubated with CCK-8 solution at 37°C for 24 h. OD values were finally evaluated using a microplate reader at 450 nm. For migration, the 24-well (pore size: 8 μ m) Transwell chamber system was used for cell migration assays. In brief, HUVECs were cultured in the serum-free RPMI-1640 medium, and 200 μ L of cell suspension was added into the upper chambers. The lower chamber was added with DMEM (Invitrogen) containing 10% FBS. After incubation for 24 h at 37°C, cells migrated to the bottom chamber and were treated with 4% paraformaldehyde fixation, 0.2% Triton X-100 treatment, and stained with 0.05% crystal violet. For tube formation assay, HUVECs were plated in the plates coated by Matrigel (300 μ L/well) at 3×10^4 cells/well. The formation of vessels-like tube structures and migrated cells was observed by using the inverted microscope (XDS-800D, Shanghai Caikang Optical Co. Ltd., China) and quantitated with the ImageJ software.

Enzyme-linked Immunosorbant Assay (ELISA)

The concentrations of homocysteine (HCy), angiotensin II (Ang II) and cardiac troponin I (cTn I) in the HUVEC supernatant and brain tissues were detected using the corresponding ELISA kits, which were purchased from Assay Genie (Ireland), Abcam (Shanghai, China), and Solarbio (Beijing, China), respectively.

Apoptosis assay

Apoptosis assay was performed using a TUNEL detection kit (cat. no. KGA702; Nanjing KeyGen Biotech Co., Ltd.). Briefly, 1×10^6 cells were permeabilized with 0.1% Triton X-100 for 30 min and incubated in 50 mM TUNEL reaction mixture for 2 h at room temperature. Each experiment was performed three times. Slides were counterstained with DAPI for 10 min at room temperature for nuclear staining. Images were captured using a fluorescence microscope (Olympus Corporation) and analyzed by the ImageJ software.

Immunofluorescence staining

The expression and distribution of HIF1 α and VEGFA were detected by immunofluorescence *in vivo* in the brain slices and *in vitro*. The thin slices of brain tissues were deparaffinized, and rehydrated and antigen retrieval was performed in citric acid buffer at PH6. The tissue slides were blocked with 5% BSA and incubated with primary antibodies for ON. The slides were washed with PBS and incubated in secondary antibodies for an hour which then treated with DAPI and mounted with mounting media (Vector# H-1200). For the *in vitro* assays, cells were seeded onto 12 mm coverslip in 24 well plates and cultured until their confluence reached about 70-80% and then fixed with 4% paraformaldehyde for 30 min at room temperature. The cells and the slides were blocked with 10% goat serum for 15 min followed by incubation with RBM24 (1:200, Abcam), HIF1 α (1:200, Abcam) or VEGFA primary antibodies overnight at 4°C. The cells or slides were incubated with FITC-conjugated secondary antibody (Thermo Fisher, 1:200) for 1 h at 37°C in the dark after washing with PBS and then counterstained with 4',6-diamidino-2-phenylindole (DAPI) (Sigma Aldrich, 0.1 μ g/ml) for 5 min. Images were taken using a fluorescent microscope.

Statistical analysis

All the statistical analyses in the present study were completed with the SPSS 21.0 software (IBM, Armonk, NY, USA). Data are shown as the mean \pm standard deviation from at least three independent experiments. Statistical comparisons were performed using unpaired *t*-test between the two groups. One-way assay of variance (ANOVA) was used to compare the differences among more than two groups. The correlation of measurements was processed with Pearson's correlation assay. $P < 0.05$ indicates statistical significance.

Results

MicroRNA microarray profiling and differentially expressed miRNAs

Among the 2549 miRNAs that were tested using the Agilent 8 \times 60 K miRNA-array platform, a total of 2134 miRNAs were found (data not shown). Of them, a total of 715 miRNAs were found to be differentially expressed

Table 1. MiR-20a-5p is significantly associated with clinicopathological characteristics of HICH.

Group	Cases	Age	Sex	Cerebral hematoma volume(mL)	NIHSS index score	BI index score
High	17	60.24±0.83	Female/male (9/8)	10.24±1.24	8.34±0.78	89.14±6.83
Low	16	59.65±0.72	Female/male (7/9)	18.34±2.13	17.14±2.83	72.67±5.12
T value		0.176	0.243	7.9	6.87	8.52
P value		0.845	0.971	< 0.001	< 0.001	< 0.001

(394 upregulated and 321 downregulated miRNAs) in the HICH patients compared to healthy individuals. MiR-20a-5p showed the most significant downregulation in HICH patients compared with healthy individuals (Figure 1A). To confirm the results, the expression of miR-20a-5p was verified in HICH patients (n=33) by qRT-PCR. As shown in Figure 1B, the expression of miR-20a-5p was significantly downregulated in HICH patients compared with healthy individuals. To elucidate the involvement of miR-20a-5p in HICH, we explored the relationship between miR-20a-5p expression and the clinicopathological characteristics of HICH. Based on miR-20a-5p expression levels, 33 patients were categorized into two groups: the miR-20a-5p high-expression group (n=17) and the low-expression group (n=16). Our findings demonstrated a significant correlation between miR-20a-5p expression and increased cerebral hematoma volume, elevated NIHSS index scores, and reduced BI index scores (refer to Table 1).

MiR-20a-5p controlled HUVEC cell proliferation, apoptosis, migration, and tube formation ability in vivo

HUVECs were transfected with miR-20a-5p mimics or inhibitors. As depicted in Figure 2A-B, the miR-20a-5p inhibitor group exhibited a significant reduction in cell proliferation and migration, while the miR-20a-5p mimics group demonstrated enhanced proliferation and migration. Similarly, tube formation ability showed inhibition in the miR-20a-5p inhibitor group and promotion in the miR-20a-5p mimics group (Fig 2C). Furthermore, apoptosis was increased in the miR-20a-5p inhibitor group and decreased in the miR-20a-5p mimics group (Figure 2D). Moreover, we observed a notable elevation in the levels of HCy, Ang II, and cTn I in the miR-20a-5p inhibitor group

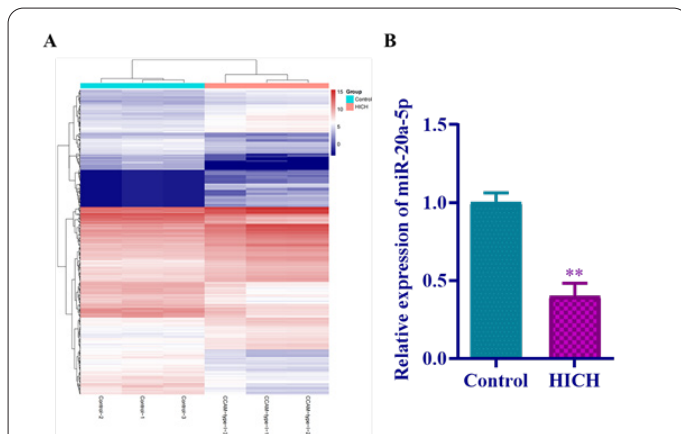


Figure 1. MicroRNA microarray profiling and differentially expressed miRNAs. (A) Heatmap presents the differentially expressed miRNAs in the HICH patients. (B) qRT-PCR analysis of miR-20a-5p in the HICH patients and control group. U6 acted as an internal control. **P < 0.01. All data are expressed as the mean ± SD.

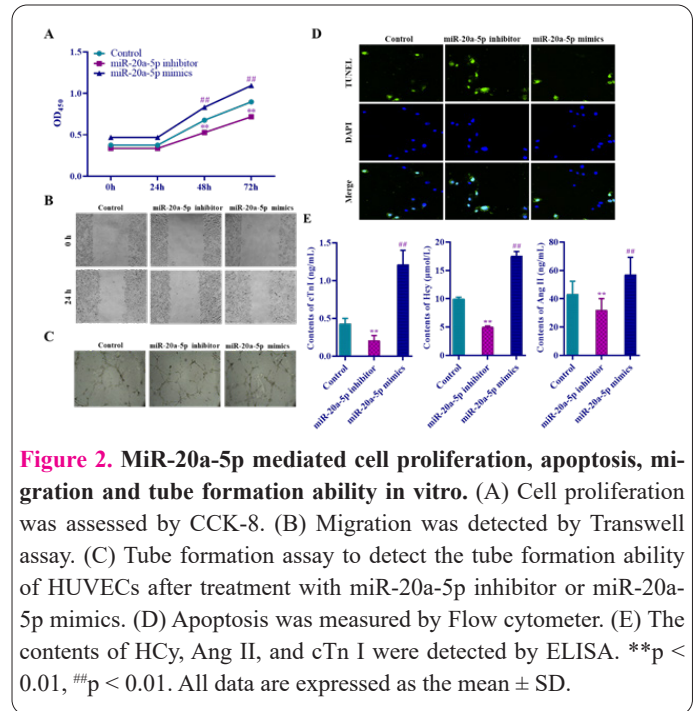


Figure 2. MiR-20a-5p mediated cell proliferation, apoptosis, migration and tube formation ability in vitro. (A) Cell proliferation was assessed by CCK-8. (B) Migration was detected by Transwell assay. (C) Tube formation assay to detect the tube formation ability of HUVECs after treatment with miR-20a-5p inhibitor or miR-20a-5p mimics. (D) Apoptosis was measured by Flow cytometer. (E) The contents of HCy, Ang II, and cTn I were detected by ELISA. **p < 0.01, ###p < 0.01. All data are expressed as the mean ± SD.

compared to the miRNA-NC group, while overexpression of miR-20a-5p led to decreased levels of HCy, Ang II, and cTn I (Figure 2E). These findings underscore the significant role of miR-20a-5p in modulating HUVEC behaviors including cell proliferation, migration, and tube formation ability.

Overexpression of miR-20a-5p inhibited HICH development in vivo

To investigate the in vivo implications of miR-20a-5p, we established a mouse model of HICH and measured blood pressure and bleeding areas. In the HICH group, the mice's blood pressure gradually increased, eventually stabilizing at approximately 180 mmHg (Figure 3A) and contained a substantial bleeding area in HICH mice (Figure 3B), affirming the successful establishment of the HICH model.

For assessing miR-20a-5p functions, we administered 20 µg of miR-20a-5p mimics or inhibitors via tail vein injection. Outcomes demonstrated blood pressure reduction in the miR-20a-5p mimic group and elevation in mice receiving the miR-20a-5p inhibitor (Figure 3C). Histological analysis showed diminished bleeding area in the miR-20a-5p mimics group, whereas the miR-20a-5p inhibitor group displayed an increased bleeding area compared to the NC group (Figure 3D). Moreover, the levels of HCy, Ang II, and cTn I were markedly reduced in the miR-20a-5p mimics group compared to the control group, while inhibition of miR-20a-5p increased HCy, Ang II, and cTn I levels (Figure 3E).

RBM24 is a direct target of miR-20a-5p

To uncover the underlying mechanism involving miR-20a-5p, potential miR-20a-5p targets were identified using TargetsCan7.2 (https://www.targetscan.org/vert_72/) (Fig 4A). Among them, carboxy-terminal domain, RNA polymerase II, polypeptide A small phosphatase-like (CTDSP-L), small phosphatase-like opioid binding protein/cell adhesion molecule-like (OPCML), and RNA binding motif protein 24 (RBM24) exhibited the highest cumulative weighted context++ scores (Fig 4B, C). Notably, RBM24 displayed the most prominent fold change and was selected for further investigation. Validating the miR-20a-5p and RBM24 relationship, a luciferase activity assay was

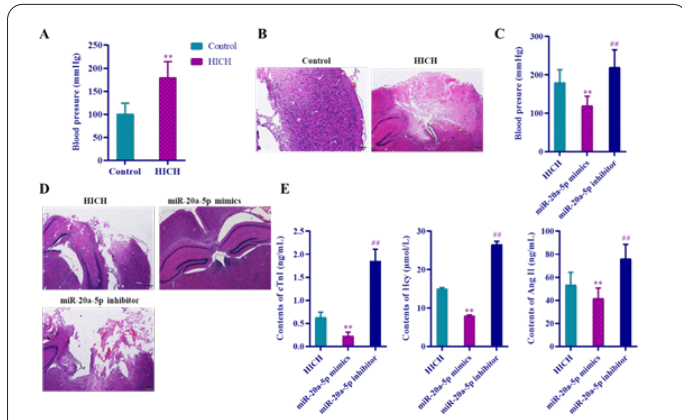


Figure 3. MiR-20a-5p suppressed development of HICH in vivo. (A) Blood pressure in HICH and control groups. (B) HE assay was performed to measure bleeding area in HICH mice. (C) Blood pressure in HICH and control groups when overexpressing or silencing miR-20a-5p. (D) H & E was conducted to reveal bleeding areas in overexpressing or silencing miR-20a-5p HICH mice. (E) The contents of Hcy, Ang II, and cTn I were detected by ELISA in overexpressing or silencing miR-20a-5p HICH mice. **p < 0.01, ##p < 0.01. All data are expressed as the mean ± SD.

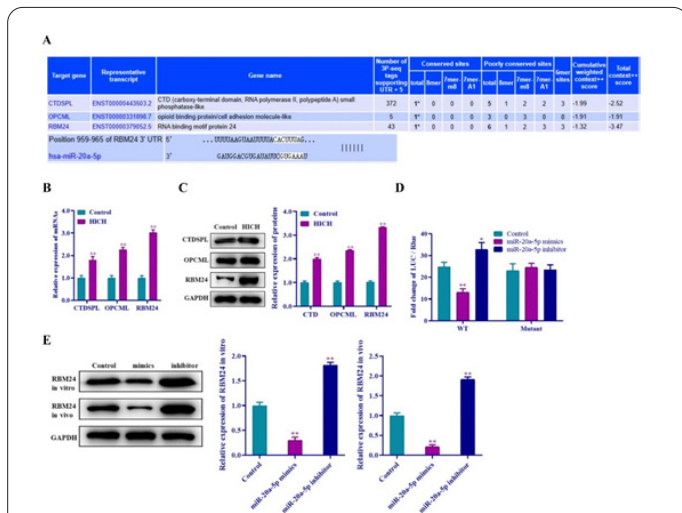


Figure 4. RBM24 is a direct target of miR-20a-5p. A) The candidate targets of miR-20a-5p were selected on TargetsCan7.2 (https://www.targetscan.org/vert_72/). (B-C) The expression levels of CTDSPL, OPCML and RBM24 were detected by qRT-PCR and Western blot. (D) Dual luciferase reporter assay to reveal the binding between RBM24 and miR-20a-5p. (E) The expression levels of RBM24 protein after treatment with miR-20a-5p mimics, miR-20a-5p inhibitor or miR NC in vitro and in vivo. GAPDH acted as the loading control. *P < 0.05, **p < 0.01, All data are expressed as the mean ± SD.

conducted in RBM24 WT and RBM24 mutant groups (Fig 4D). The results indicated that luciferase activity in the RBM24 WT group significantly diminished in the presence of miR-20a-5p mimics, while it increased with the presence of its inhibitor. Remarkably, negligible changes were observed in any subgroup of the RBM24 Mutant group, demonstrating miR-20a-5p's specific targeting and inhibition of RBM24. Additionally, in vivo, and in vitro western blot data reflected reduced RBM24 expression upon miR-20a-5p mimic presence. In vivo data from mice demonstrated miR-20a-5p inhibitor upregulating RBM24 expression, while miR-20a-5p mimics significantly decreased RBM24 expression in HUVECs and brain tissues of HICH mice (Figure 4E). These results collectively underscore RBM24 as a direct miR-20a-5p target through 3'UTR binding.

MiR-20a-5p suppressed the development of HICH by downregulation of RBM24

Subsequently, a gain and loss of function assay was conducted to further dissect RBM24's role in HICH development. Elevating RBM24 expression in HUVECs resulted in suppressed cell proliferation, migration, and tube formation ability, whereas RBM24 silencing yielded converse effects (Figure 5A-C). Moreover, cell apoptosis was notably augmented in the RBM24 overexpression group and hindered in the RBM24 suppression group (Figure 5D). For in vivo evaluation of RBM24's function, lentivirus carrying the full-length RBM24 and si-RNA targeting RBM24 were introduced into mice via tail vein injection. The findings revealed heightened blood pressure in RBM24-overexpressing mice, whereas blood pressure decreased in the RBM24-suppressed group (Figure 5E). Additionally, the bleeding area expanded in the RBM24 overexpression group and contracted in the RBM24 downregulation group compared to the HICH group (Figure 5F). Furthermore, elevated levels of Hcy, Ang II, and cTn I were evident in the RBM24 upregulation group, while RBM24 suppression led to decreased Hcy, Ang II, and cTn I contents in Ang II-stimulated HUVECs and mice brain tissues (Figure 5G and H). Notably, rescue experiments underscored RBM24 silencing's reversal of miR-20a-5p inhibitor effects on HUVEC proliferation, migration, tube formation ability, and apoptosis, implying miR-20a-5p's action via RBM24 inhibition (Figure 5I-L).

MiR-20a-5p repressed the development of HICH depending on HIF1α/VEGFA pathway

The significance of the HIF1α/VEGFA axis in angiogenesis across various diseases (18-20) including intracerebral hemorrhage (17,21) is well documented. Studies have revealed miR-20a-5p's role in suppressing tumor angiogenesis in non-small cell lung cancer (22). Consequently, we hypothesized that miR-20a-5p might influence the HIF1α/VEGFA signaling pathway in our animal model.

To ascertain the association between the miR-20a-5p-RBM24 axis and the HIF1α/VEGFA pathway in HICH development, we examined HIF1α and VEGFA expression levels in HUVECs and our mouse HICH model. The results indicated that in Ang II-stimulated HUVECs overexpressing RBM24, both protein and mRNA levels of HIF1α/VEGFA were significantly diminished (Figure 6A-C) compared to control groups. However, the expression levels were partly restored, at the very least, in the

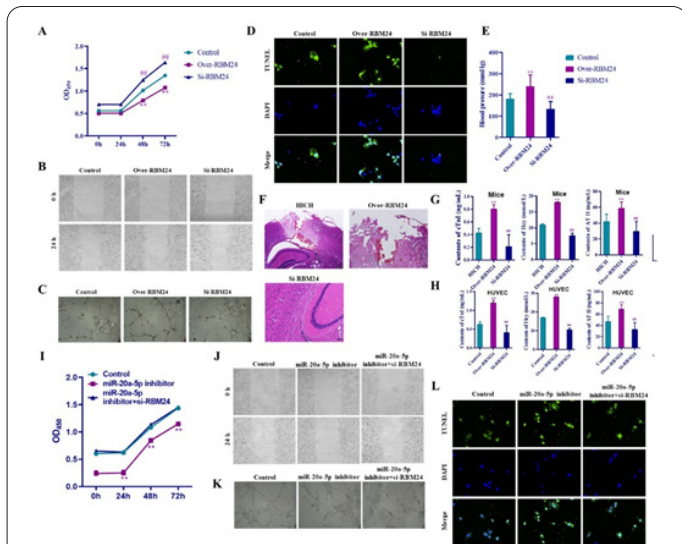


Figure 5. MiR-20a-5p hindered the development of HICH by downregulation of RBM24. (A) Cell proliferation was measured by CCK-8 when overexpressing or silencing RBM24 in vitro. (B) Migration was detected by transwell assay when overexpressing or silencing RBM24 in vitro. (C) Tube formation assay to detect the tube formation ability of HUVECs when overexpressing or silencing RBM24. (D) Apoptosis was measured by TUNEL assay in HUVECs overexpressing or silencing RBM24. (E) Blood pressure in mice of the HICH and control groups when overexpressing or silencing RBM24. (F) HE assay was conducted to reveal the bleeding area in mice overexpressing or silencing RBM24. (G-H) The contents of Hcy, Ang II, and cTn I were detected by ELISA kits in HICH mice and HUVECs overexpressing or silencing RBM24. (I) Cell proliferation was assessed by CCK-8 in miR-20a-5p inhibitor group rescued by silenced RBM24 in vitro. (J) Migration was detected by Transwell assay in miR-20a-5p inhibitor group rescued by silenced RBM24 in vitro. (K) Tube formation assay to detect the angiogenic ability of HUVECs in miR-20a-5p inhibitor group rescued by silenced RBM24 in vitro. (L) Apoptosis was measured by TUNEL assay in miR-20a-5p inhibitor group rescued by silenced RBM24 in vitro. **p < 0.01, ##p < 0.01. All data are expressed as the mean ± SD.

compared to healthy individuals, exhibiting notable associations with clinicopathological attributes of HICH. Our subsequent analyses unveiled the regulatory role of the miR-20a-5p/RBM24 axis in HICH through modulation of the HIF1α/VEGFA signaling pathway. This insight could hold significance for augmenting endogenous miR-20a-5p expression, thus impacting the diagnosis and treatment of HICH.

The triad of developmental anomalies in the middle arterial wall layer, arteriosclerosis, and hypertension stands as pivotal factors in cerebral hemorrhage, where hypertension remains an important independent risk element (23).

Although the exact etiology of HICH remains incompletely understood, hypertension is widely acknowledged as a cornerstone. Mechanical stresses resulting from hypertension impinge on endothelial cells (ECs), culminating in a sequence of pathological changes that compromise vascular wall integrity (24).

Nevertheless, the molecular underpinnings of HICH remain less explored. MiRNAs play a central role in various biological processes, including cell proliferation, differentiation, and metabolism (25). Some miRNAs have been implicated in intracerebral hemorrhage, such as miR-124, miR-340-5p, and miR-26a-5p (26-28).

Yet, limited attention has been devoted to miRNAs in the context of HICH. Herein, our study unveiled 715 differentially expressed miRNAs in HICH patients through miRNA microarray analysis. Among them, miR-20a-5p emerged as significantly downregulated in HICH patients compared to healthy individuals, with distinct associations to clinicopathological characteristics of HICH. This emphasizes miR-20a-5p's consequential role in HICH. Notably, miR-20a-5p has been shown to inhibit epithelial-to-mesenchymal transition and impede endometrial cancer cell invasion by targeting STAT3 (29). Additionally, recent findings demonstrated miR-20a-5p's suppression of tumor angiogenesis in non-small cell lung cancer through the RRM2-mediated PI3K/Akt pathway (22). Consistent-

presence of miR-20a-5p mimics. Similarly, in assessing RBM24's function, lentivirus carrying the full-length RBM24 was introduced into mice. The outcomes revealed reduced HIF1α and VEGFA levels at the protein and mRNA levels in response to elevated RBM24 levels, an effect that was reversed by the presence of miR-20a-5p mimic compared to HICH controls (Figure 6D-F). This suggests that the influence of miR-20a-5p on the HIF1α/VEGF-A pathway is contingent upon RBM24.

Discussion

Surgical intervention alone often falls short in yielding satisfactory outcomes for HICH patients due to the challenging deep-seated location of the brain tissue bleed. With its rapid onset, high disability rate, and elevated fatality rate, HICH imposes a substantial burden on individuals, families, and society at large. Thus, there is a pressing need to identify effective biomarkers and conduct comprehensive investigations into their roles in HICH pathogenesis, targeted therapy, and prognosis.

In this study, we delved into differentially expressed miRNAs in HICH. Among them, miR-20a-5p emerged as the most significantly downregulated in HICH patients

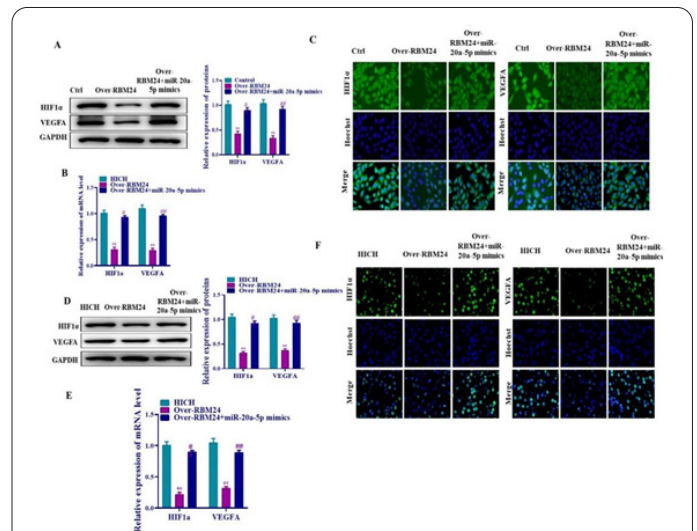


Figure 6. MiR-20a-5p hindered the development of HICH depending on HIF1α/VEGFA pathway. The expression of HIF1α and VEGFA was measured by qRT-PCR, western blot, and immunofluorescence staining after RBM24 overexpression or suppression in HUVECs (A-C) and in HICH mice (D-F). GAPDH acted as an internal control for qRT-PCR and western blot. The relative grey density was calculated by the ImageJ software. **p < 0.01, ###p < 0.01. All data are expressed as the mean ± SD.

ly, our study highlighted that miR-20a-5p downregulation bolstered cell proliferation, migration, and tube formation ability, while abating apoptosis *in vitro*, and mitigated HICH development *in vivo*, collectively implicating miR-20a-5p's inhibitory impact on angiogenesis.

The regulatory interplay of miRNAs with target mRNA through 3'UTR binding is well-established across diverse diseases. In this study, we pinpointed RBM24 as a direct target of miR-20a-5p. RBM24 has demonstrated pivotal roles in diverse processes across multiple diseases, including cell alternative splicing, lung cancer progression, and skeletal muscle regeneration (30,31).

Notably, RBM24 itself is a target of miRNAs, as exemplified by miR-222's modulation of muscle alternative splicing via Rbm24 during skeletal muscle cell differentiation (32). RBM24 restoration has been shown to suppress nasopharyngeal carcinoma cell proliferation, migration, invasion, and metastatic colonization by upregulating miR-25 (33). In our study, RBM24 overexpression inhibited HUVEC cell proliferation, migration, and tube formation ability, while enhancing apoptosis *in vitro*, and exacerbated HICH development *in vivo*. Furthermore, silencing RBM24 partially rescued the inhibitory effects of miR-20a-5p on HICH, both *in vivo* and *in vitro*. These findings underscore miR-20a-5p's regulatory role in HICH through the suppression of RBM24 expression.

The HIF1 α /VEGFA axis has been widely recognized as pivotal for angiogenesis in various diseases, encompassing intracerebral hemorrhage (17-21). Specifically, the HIF1 α gene plays a role in enhancing the proliferation, migration, and differentiation of endogenous neural stem cells post-ICH, thereby contributing to neurofunctional recovery (34). HIF1 α , along with its downstream pathways, has been demonstrated to mitigate neuronal injury after intracerebral hemorrhage in the context of diabetes (35). Notably, Cui et al. recently demonstrated that thrombin-induced elevation of miR-24, which targets PHD1, stabilizes HIF1 α and triggers angiogenesis post-ICH, hinting at HIF1 α 's involvement in HICH regulation (16).

In our study, we established that the expression of HIF1 α and VEGFA was significantly diminished in Ang II-stimulated HUVECs and mice, as compared to the control group. Further investigations revealed that RBM24 overexpression inhibited HIF1 α and VEGFA expression, while miR-20a-5p reversed these changes. This suggests that miR-20a-5p's impact on the HIF1 α /VEGFA pathway is contingent upon RBM24. Collectively, our findings highlight the regulatory role of the miR-20a-5p/RBM24 axis in HICH via modulation of the HIF1 α /VEGFA signaling pathway. This opens avenues for further exploration of miR-20a-5p's potential as a therapeutic target for HICH.

Our study demonstrates that miR-20a-5p exhibits significant downregulation in HICH patients compared to healthy individuals, and its levels correlate with clinicopathological characteristics of HICH. Further investigations reveal that the miR-20a-5p/RBM24 axis modulates HICH progression by influencing the HIF1 α /VEGFA signaling pathway. These findings provide a robust foundation for advancing preventive strategies against the occurrence and progression of HICH.

Ethical approval

The study was approved by the ethics committee of Nanjing Pukou People's Hospital under permission num-

ber PKU-239943789.

Competing interests

We have no competing interests.

Funding

This work was supported by the Pukou district social science and technology planning project of 2018 (No. s2018-05), the Science and Technology Development Fund of PuKou Branch Hospital of Jiangsu Province Hospital (No. KJ2021-7).

Availability of data and materials

Complete data obtained during this study has been included in this manuscript.

References

1. Ueno M. [Hypertensive cerebral hemorrhage]. *Nihon Rinsho* 2004;62 Suppl 3:363-368.
2. Fisher CM. Hypertensive cerebral hemorrhage. Demonstration of the source of bleeding. *J Neuropathol Exp Neurol* 2003;62(1):104-107. doi:10.1093/jnen/62.1.104
3. Ding W, Gu Z, Song D, Liu J, Zheng G, Tu C. Development and validation of the hypertensive intracerebral hemorrhage prognosis models. *Medicine (Baltimore)* 2018;97(39):e12446. doi:10.1097/MD.00000000000012446
4. Gavito-Higuera J, Khatri R, Qureshi IA, Maud A, Rodriguez GJ. Aggressive blood pressure treatment of hypertensive intracerebral hemorrhage may lead to global cerebral hypoperfusion: Case report and imaging perspective. *World J Radiol* 2017;9(12):448-453. doi:10.4329/wjr.v9.i12.448
5. Heinzel J, Längle G, Oberhauser V, et al. Use of the CatWalk gait analysis system to assess functional recovery in rodent models of peripheral nerve injury - a systematic review. *J Neurosci Methods* 2020;345:108889. doi:10.1016/j.jneumeth.2020.108889
6. Zia E, Hedblad B, Pessah-Rasmussen H, Berglund G, Janzon L, Engstrom G. Blood pressure in relation to the incidence of cerebral infarction and intracerebral hemorrhage. *Hypertensive hemorrhage: debated nomenclature is still relevant. Stroke* 2007;38(10):2681-2685. doi:10.1161/STROKEAHA.106.479725
7. Lei C, Wu B, Liu M, Cao T, Wang Q, Dong W. Differences Between Vascular Structural Abnormality and Hypertensive Intracerebral Hemorrhage. *J Stroke Cerebrovasc Dis* 2015;24(8):1811-1816. doi:10.1016/j.jstrokecerebrovasdis.2015.04.006
8. Tian DZ, Wei W, Dong YJ. Influence of COL1A2 gene variants on the incidence of hypertensive intracerebral hemorrhage in a Chinese population. *Genet Mol Res* 2016;15(1). doi:10.4238/gmr.15017369
9. Liu J, Gao DY, Li JN. Correlations of endothelin-1 gene polymorphisms and hypertensive intracerebral hemorrhage. *Eur Rev Med Pharmacol Sci* 2020;24(22):11776-11782. doi:10.26355/eur-rev_202011_23832
10. Mendell JT. MicroRNAs: critical regulators of development, cellular physiology and malignancy. *Cell Cycle* 2005;4(9):1179-1184. doi:10.4161/cc.4.9.2032
11. Bartel DP. MicroRNAs: genomics, biogenesis, mechanism, and function. *Cell* 2004;116(2):281-297. doi:10.1016/s0092-8674(04)00045-5
12. Weldon Furr J, Morales-Scheihing D, Manwani B, Lee J, McCullough LD. Cerebral Amyloid Angiopathy, Alzheimer's Disease and MicroRNA: miRNA as Diagnostic Biomarkers and Potential Therapeutic Targets. *Neuromolecular Med* 2019;21(4):369-390. doi:10.1007/s12017-019-08568-0

13. Gareev IF, Safin SM. [The role of endogenous miRNAs in the development of cerebral aneurysms]. *Zh Vopr Neurokhir Im N N Burdenko* 2019;83(1):112-118. doi:10.17116/neiro201983011112
14. Li L, Wang P, Zhao H, Luo Y. Noncoding RNAs and Intracerebral Hemorrhage. *CNS Neurol Disord Drug Targets* 2019;18(3):205-211. doi:10.2174/1871527318666190204102604
15. Chen JX, Wang YP, Zhang X, Li GX, Zheng K, Duan CZ. LncRNA Mtss1 promotes inflammatory responses and secondary brain injury after intracerebral hemorrhage by targeting miR-709 in mice. *Brain Res Bull* 2020;162:20-29. doi:10.1016/j.brainresbull.2020.04.017
16. Cui H, Yang A, Zhou H, et al. Thrombin-induced miRNA-24-1-5p upregulation promotes angiogenesis by targeting prolyl hydroxylase domain 1 in intracerebral hemorrhagic rats. *J Neurosurg* 2020:1-12. doi:10.3171/2020.2.JNS193069
17. Dong B, Zhou B, Sun Z, et al. LncRNA-FENDRR mediates VEGFA to promote the apoptosis of brain microvascular endothelial cells via regulating miR-126 in mice with hypertensive intracerebral hemorrhage. *Microcirculation* 2018;25(8):e12499. doi:10.1111/micc.12499
18. Wan J, Wu W, Chen Y, Kang N, Zhang R. Insufficient radiofrequency ablation promotes the growth of non-small cell lung cancer cells through PI3K/Akt/HIF-1alpha signals. *Acta Biochim Biophys Sin (Shanghai)* 2016;48(4):371-377. doi:10.1093/abbs/gmw005
19. Liang H, Xiao J, Zhou Z, et al. Hypoxia induces miR-153 through the IRE1alpha-XBP1 pathway to fine tune the HIF1alpha/VEGFA axis in breast cancer angiogenesis. *Oncogene* 2018;37(15):1961-1975. doi:10.1038/s41388-017-0089-8
20. Wang J, Man GCW, Chan TH, Kwong J, Wang CC. A prodrug of green tea polyphenol (-)-epigallocatechin-3-gallate (Pro-EGCG) serves as a novel angiogenesis inhibitor in endometrial cancer. *Cancer Lett* 2018;412:10-20. doi:10.1016/j.canlet.2017.09.054
21. Chen ZQ, Yu H, Li HY, et al. Negative regulation of glial Tim-3 inhibits the secretion of inflammatory factors and modulates microglia to antiinflammatory phenotype after experimental intracerebral hemorrhage in rats. *CNS Neurosci Ther* 2019;25(6):674-684. doi:10.1111/cns.13100
22. Han J, Hu J, Sun F, Bian H, Tang B, Fang X. MicroRNA-20a-5p suppresses tumor angiogenesis of non-small cell lung cancer through RRM2-mediated PI3K/Akt signaling pathway. *Mol Cell Biochem* 2020. doi:10.1007/s11010-020-03936-y
23. Ishisaka T, Igarashi Y, Kodera K, et al. Relationship Between Blood Pressure Levels on Admission and the Onset of Acute Pneumonia in Elderly Patients With Cerebral Hemorrhage. *J Clin Med Res* 2020;12(11):693-698. doi:10.14740/jocmr4330
24. Pasi M, Sugita L, Xiong L, et al. Association of cerebral small vessel disease and cognitive decline after intracerebral hemorrhage. *Neurology* 2020. doi:10.1212/WNL.0000000000011050
25. Grillari J, Makitie RE, Kocijan R, et al. Circulating miRNAs in bone health and disease. *Bone* 2020:115787. doi:10.1016/j.bone.2020.115787
26. Bao WD, Zhou XT, Zhou LT, et al. Targeting miR-124/Ferroportin signaling ameliorated neuronal cell death through inhibiting apoptosis and ferroptosis in aged intracerebral hemorrhage murine model. *Aging Cell* 2020;19(11):e13235. doi:10.1111/accel.13235
27. Zhou W, Huang G, Ye J, Jiang J, Xu Q. Protective Effect of miR-340-5p against Brain Injury after Intracerebral Hemorrhage by Targeting PDCD4. *Cerebrovasc Dis* 2020;49(6):593-600. doi:10.1159/000508210
28. Zhang H, Lu X, Hao Y, Tang L, He Z. MicroRNA-26a-5p alleviates neuronal apoptosis and brain injury in intracerebral hemorrhage by targeting RAN binding protein 9. *Acta Histochem* 2020;122(5):151571. doi:10.1016/j.acthis.2020.151571
29. Huang Y, Yang N. MicroRNA-20a-5p inhibits epithelial to mesenchymal transition and invasion of endometrial cancer cells by targeting STAT3. *Int J Clin Exp Pathol* 2018;11(12):5715-5724.
30. Zhang D, Ma Y, Ma Z, et al. Circular RNA SMARCA5 suppressed non-small cell lung cancer progression by regulating miR-670-5p/RBM24 axis. *Acta Biochim Biophys Sin (Shanghai)* 2020;52(10):1071-1080. doi:10.1093/abbs/gmaa099
31. Zhang M, Han Y, Liu J, et al. Rbm24 modulates adult skeletal muscle regeneration via regulation of alternative splicing. *Theranostics* 2020;10(24):11159-11177. doi:10.7150/thno.44389
32. Cardinali B, Cappella M, Provenzano C, et al. MicroRNA-222 regulates muscle alternative splicing through Rbm24 during differentiation of skeletal muscle cells. *Cell Death Dis* 2016;7:e2086. doi:10.1038/cddis.2016.10
33. Hua WF, Zhong Q, Xia TL, et al. RBM24 suppresses cancer progression by upregulating miR-25 to target MALAT1 in nasopharyngeal carcinoma. *Cell Death Dis* 2016;7(9):e2352. doi:10.1038/cddis.2016.252
34. Yu Z, Chen LF, Tang L, Hu CL. Effects of recombinant adenovirus-mediated hypoxia-inducible factor-1alpha gene on proliferation and differentiation of endogenous neural stem cells in rats following intracerebral hemorrhage. *Asian Pac J Trop Med* 2013;6(10):762-767. doi:10.1016/S1995-7645(13)60134-0
35. Yu Z, Tang L, Chen L, Li J, Wu W, Hu C. Role for HIF-1alpha and Downstream Pathways in Regulating Neuronal Injury after Intracerebral Hemorrhage in Diabetes. *Cell Physiol Biochem* 2015;37(1):67-76. doi:10.1159/000430334